AGING

A programmable fate decision landscape underlies single-cell aging in yeast

Yang Li[1], Yanfei Jiang[1], Julie Paxman[1], Richard O'Laughlin[2], Stephen Klepin[1], Yuelian Zhu[1], Lorraine Pillus[1,3], Lev S. Tsimring[4], Jeff Hasty[1,2,4], Nan Hao[1,4]*

Chromatin instability and mitochondrial decline are conserved processes that contribute to cellular aging. Although both processes have been explored individually in the context of their distinct signaling pathways, the mechanism that determines which process dominates during aging of individual cells is unknown. We show that interactions between the chromatin silencing and mitochondrial pathways lead to an epigenetic landscape of yeast replicative aging with multiple equilibrium states that represent different types of terminal states of aging. The structure of the landscape drives single-cell differentiation toward one of these states during aging, whereby the fate is determined quite early and is insensitive to intracellular noise. Guided by a quantitative model of the aging landscape, we genetically engineered a long-lived equilibrium state characterized by an extended life span.

Many damage factors, including chromatin instability, mitochondrial dysfunction, and reactive oxygen species (*1*, *2*), contribute to cellular aging. In each individual cell, how these factors combine to drive the aging process remains unclear. For instance, aging could be driven by independent damage mechanisms that accumulate at varying rates, resulting in different aged phenotypes in individual cells, or, alternatively, by the deterioration of overall cellular condition, leading to a common aging pathway in all cells. Single-cell analysis can reveal which scenario actually underlies the aging process. We investigated replicative aging of the yeast *Saccharomyces cerevisiae*, a genetically tractable model for the aging of mitotic cell types such as stem cells (*3*, *4*). Yeast aging research has focused on life span, as measured by the number of cell divisions before death (*5*). We integrated microfluidics (fig. S1) with time-lapse microscopy to measure life span along with dynamic changes of gene expression, chromatin state, and organelle morphology, enabling us to reveal a long-lived mode of the single-cell aging process in yeast.

We found that isogenic wild-type (WT) cells exhibited two types of phenotypic changes during aging (*6*, *7*). About half of cells produced daughters with an elongated morphology during later stages of their life span. In contrast, the other half continuously produced small, round daughter cells until death. We designate these phenotypic changes as "mode 1" and "mode 2" aging, respectively (Fig. 1A and figs. S2 and S3). Aberrant structural changes of the nucleolus and mitochondria are hallmarks of aging in many organisms, indicating age-associated organellar dysfunction (*8*, *9*). Nucleoli were enlarged and fragmented in all mode 1 aged cells but not in mode 2 cells (Fig. 1B, top, and fig. S4). Mitochondria in mode 1 cells, however, retained a normal tubular morphology throughout life, whereas those in mode 2 became aggregated before cell death (Fig. 1B, bottom), in accord with mitochondrial decline observed previously in a fraction of cells (*10*). Thus, the two aging modes were associated with distinct organellar failures: mode 1 with nucleolar decline and mode 2 with mitochondrial decline.

Age-dependent nucleolar enlargement is related to instability of ribosomal DNA (rDNA) (*11*, *12*). The conserved lysine deacetylase Sir2, encoded by a well-studied longevity gene, maintains rDNA stability by mediating rDNA silencing (*13*). To track rDNA silencing, we used a green fluorescent protein (GFP) reporter inserted at the nontranscribed spacer region of rDNA (rDNA-GFP) (*6*). Expression of the reporter is repressed by silencing, so increased fluorescence indicates a loss of silencing. Cells exhibited sporadic loss of silencing during early phases of aging (*6*). Late in aging, mode 1 cells underwent sustained loss of silencing, but mode 2 cells did not (Fig. 1C), in accord with nucleolar decline only in mode 1 cells. Exposure to nicotinamide (NAM), a Sir2 inhibitor that disrupts rDNA silencing, induced mode 1 aging in most cells (fig. S5A), suggesting a role of Sir2 and rDNA silencing in driving mode 1 aging. NAM treatment can also lead to elongated cell morphology, which may be a consequence of loss of Sir2 activity (fig. S5B).

For mode 2 aging, we monitored heme, an iron-containing compound proposed to be a key factor for mitochondrial decay during human aging (*14*). To determine how heme abundance changed during aging, we used two independent reporters: a fluorescent HS1 heme sensor (*15*) and a nuclear anchored infrared fluorescent protein reporter (nuc. iRFP) (*16*). For HS1, because binding of heme to its receptor quenches GFP fluorescence, increased GFP signal indicates decreased heme. For nuc. iRFP, fluorescence depends on a product of heme catabolism, biliverdin, and was found to correlate with the amount of cellular heme (fig. S6). These two reporters, expressed in the same cells, showed consistently that the amount of heme decreased in mode 2 aging but not mode 1 aging (Fig. 1D). Heme activates the heme activator protein (HAP) transcriptional complex to maintain mitochondrial biogenesis and function (*17*). Consistently, expression of HAP-regulated genes *COX5a* and *CYC1*, both of which encode key mitochondrial components, decreased specifically in mode 2 cells (figs. S7 and S8). Depletion of heme by succinylacetone induced mode 2 aging in most cells (fig. S5C), indicating that the decrease in heme abundance and HAP activity may drive mode 2 aging. Heme depletion also coincided with increased abundance of the plasma membrane proton pump Pma1 (fig. S9), which causes decreased vacuolar acidity and mitochondrial dysfunction during aging (*9*, *18*, *19*). Moreover, mode 2 aging featured a shorter life span and a greater extension of cell cycle length than mode 1 aging (Fig. 1, E and F).

To track rDNA silencing and heme abundance simultaneously, we introduced rDNA-GFP and nuc. iRFP reporters into the same cells. Newborn cells began with relatively uniform amounts of the two reporters and diverged in two opposite directions during the early half of their lifetimes. Mode 1 cells (47.3% of the population) ended life with high GFP and high iRFP signals, corresponding to a state with low rDNA silencing and a high abundance of heme. In contrast, mode 2 cells (52.7% of the population) ended in a state with high rDNA silencing and a low abundance of heme (Fig. 1G, fig. S10, and movie S1). Thus, isogenic cells age toward two discrete terminal states with anticorrelated rDNA silencing and heme abundance, suggesting interactions between these pathways.

To test for such an interaction, we deleted *SIR2* to disrupt rDNA silencing in the dual reporter strain. The majority (83.1%) of *sir2*Δ cells showed increased iRFP fluorescence during aging, consistent with increased heme abundance and HAP activity in the absence of Sir2 (Fig. 2A). The expression of HAP-regulated genes *COX5a* and *CYC1* was also increased in *sir2*Δ cells (fig. S11). The majority (83.1%) of *sir2*Δ cells aged with mode 1 phenotypes. Whereas WT mode 1 cells lost silencing at a late phase of aging, *sir2*Δ cells showed sustained loss of rDNA silencing throughout their lives, resulting in accelerated progression toward death (fig. S12) (*6*). When *HAP4*, which encodes

[1]Section of Molecular Biology, Division of Biological Sciences, University of California San Diego, La Jolla, CA 92093, USA. [2]Department of Bioengineering, University of California San Diego, La Jolla, CA 92093, USA. [3]UCSD Moores Cancer Center, University of California San Diego, La Jolla, CA 92093, USA. [4]BioCircuits Institute, University of California San Diego, La Jolla, CA 92093, USA.
*Corresponding author. Email: nhao@ucsd.edu

a major component of the HAP complex, was deleted, 89.8% of cells showed decreased rDNA-GFP fluorescence during aging, consistent with increased rDNA silencing in the absence of HAP (Fig. 2B). The majority (89.8%) of *hap4*Δ cells aged with mode 2 phenotypes and quickly approached a state with high rDNA silencing and a low abundance of heme before death.

When Hap4 expression was increased, 95.9% of cells showed decreased rDNA silencing during aging and aged with mode 1 phenotypes, consistent with an inhibition of Sir2 by HAP during aging (Fig. 2C and fig. S13). Caloric restriction (CR), which induces Hap4 expression (*20*, *21*), also increased the proportion of mode 1 cells (fig. S14). In contrast, twofold overexpression of Sir2 (fig. S15) increased the proportion of mode 2 cells with decreased heme abundance, in agreement with Sir2-mediated inhibition of HAP. Additionally, Sir2

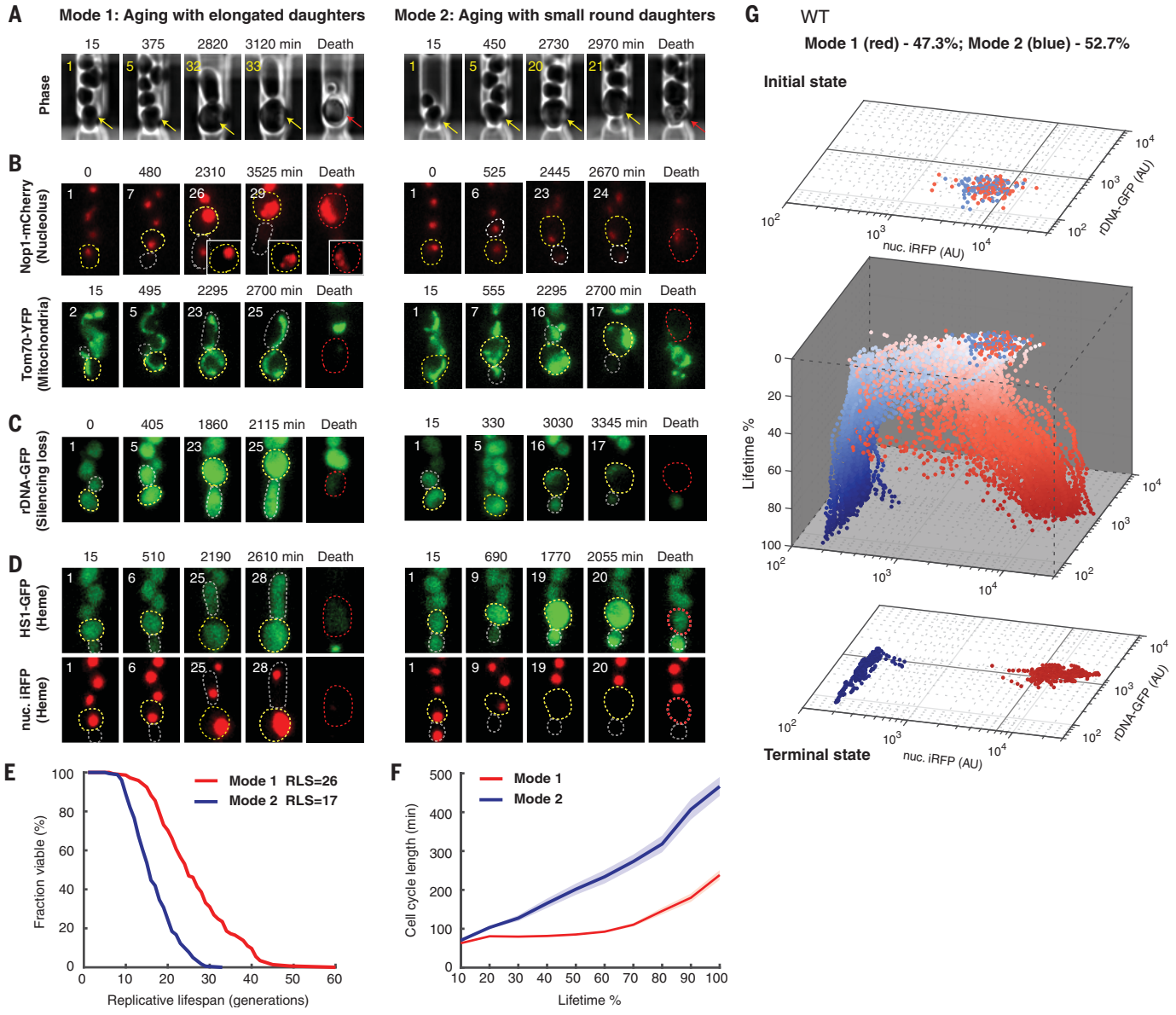

Fig. 1. Sir2 and HAP mediate divergent aging of isogenic cells. Representative time-lapse images of mode 1 and mode 2 aging processes, for (**A**) phase (n = 187 cells); (**B**) Nop1-mCherry (nucleolar marker; n = 116) and Tom70-YFP (mitochondrial marker; n = 142); (**C**) rDNA-GFP (n = 256); and (**D**) HS1-GFP and nuc. iRFP (heme reporters in the same cells; n = 230). Time-lapse images are representative of all mode 1 and mode 2 cells measured in this study. Replicative age of the mother cell is shown at the top left corner of each image. For phase images, aging and dead mother cells are marked by yellow and red arrows, respectively. In fluorescence images, aging mother cells, newborn daughter cells, and dead mother cells are circled in yellow, gray, and red, respectively. Images in Nop1-mCherry insets use different contrast to illustrate nucleolar fragmentation. (**E**) Replicative life spans (RLSs) of mode 1 and mode 2 cells (P < 0.0001, log-rank test; P < 0.0001, Gehan-Breslow-Wilcoxon test). (**F**) Changes of cell cycle length during mode 1 (red) and mode 2 (blue) aging (mode 1: n = 89; mode 2: n = 99). Shaded areas represent standard errors of the mean (SEM). (**G**) Aging trajectories of a population of WT cells (n = 187). Initial states of all the cells are projected onto a rDNA-GFP versus nuc. iRFP plane. The three-dimensional space shows the aging processes of all cells, in which the z axis represents the percentage of lifetime. Each dot represents quantified rDNA-GFP and nuc. iRFP fluorescence in a single cell at a given moment (mode 1, red; mode 2, blue). Terminal states of all the cells are projected onto another rDNA-GFP versus nuc. iRFP plane. Experiments were independently performed at least three times. AU, arbitrary units.

overexpression generated a third mode of aging, one that ended with high rDNA silencing and high heme abundance (Fig. 2D). Cells undergoing this mode of aging (mode 3) were long-lived (Fig. 2E), and they differed from mode 1 cells in that, although they also produced elongated daughters, their cell cycle lengths were unchanged throughout their life spans (Fig. 2F, fig. S16, and movie S2).

To analyze the mechanisms underlying divergent aging, we devised a model composed of two ordinary differential equations incorporating the proposed mutual inhibition between Sir2 and HAP as well as positive autoregulation of each (Fig. 3A). The mutual inhibition may act through transcriptional regulation, as the transcription of many HAP components and HAP-regulated genes is

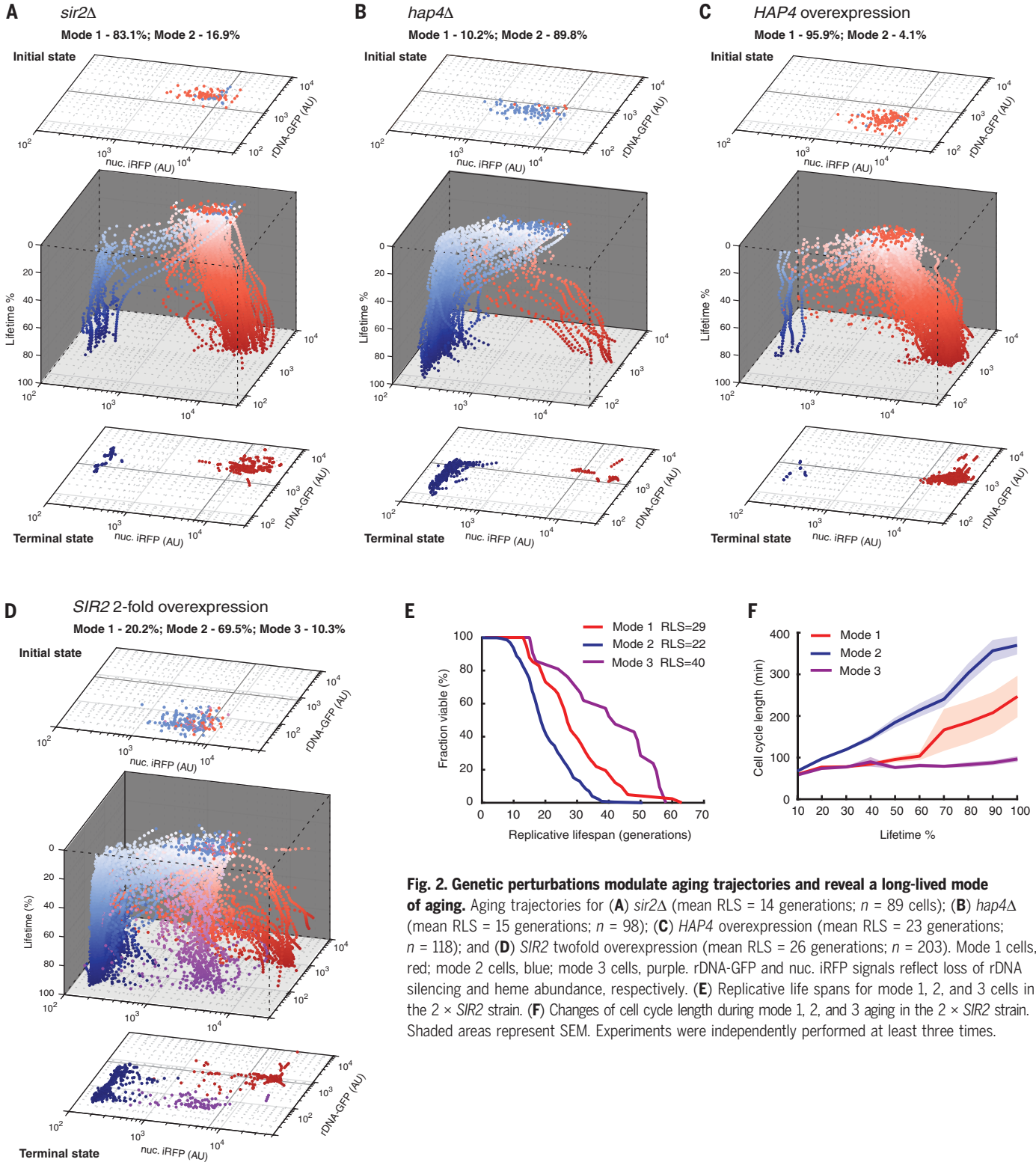

Fig. 2. Genetic perturbations modulate aging trajectories and reveal a long-lived mode of aging. Aging trajectories for (**A**) *sir2*Δ (mean RLS = 14 generations; *n* = 89 cells); (**B**) *hap4*Δ (mean RLS = 15 generations; *n* = 98); (**C**) *HAP4* overexpression (mean RLS = 23 generations; *n* = 118); and (**D**) *SIR2* twofold overexpression (mean RLS = 26 generations; *n* = 203). Mode 1 cells, red; mode 2 cells, blue; mode 3 cells, purple. rDNA-GFP and nuc. iRFP signals reflect loss of rDNA silencing and heme abundance, respectively. (**E**) Replicative life spans for mode 1, 2, and 3 cells in the 2 × *SIR2* strain. (**F**) Changes of cell cycle length during mode 1, 2, and 3 aging in the 2 × *SIR2* strain. Shaded areas represent SEM. Experiments were independently performed at least three times.

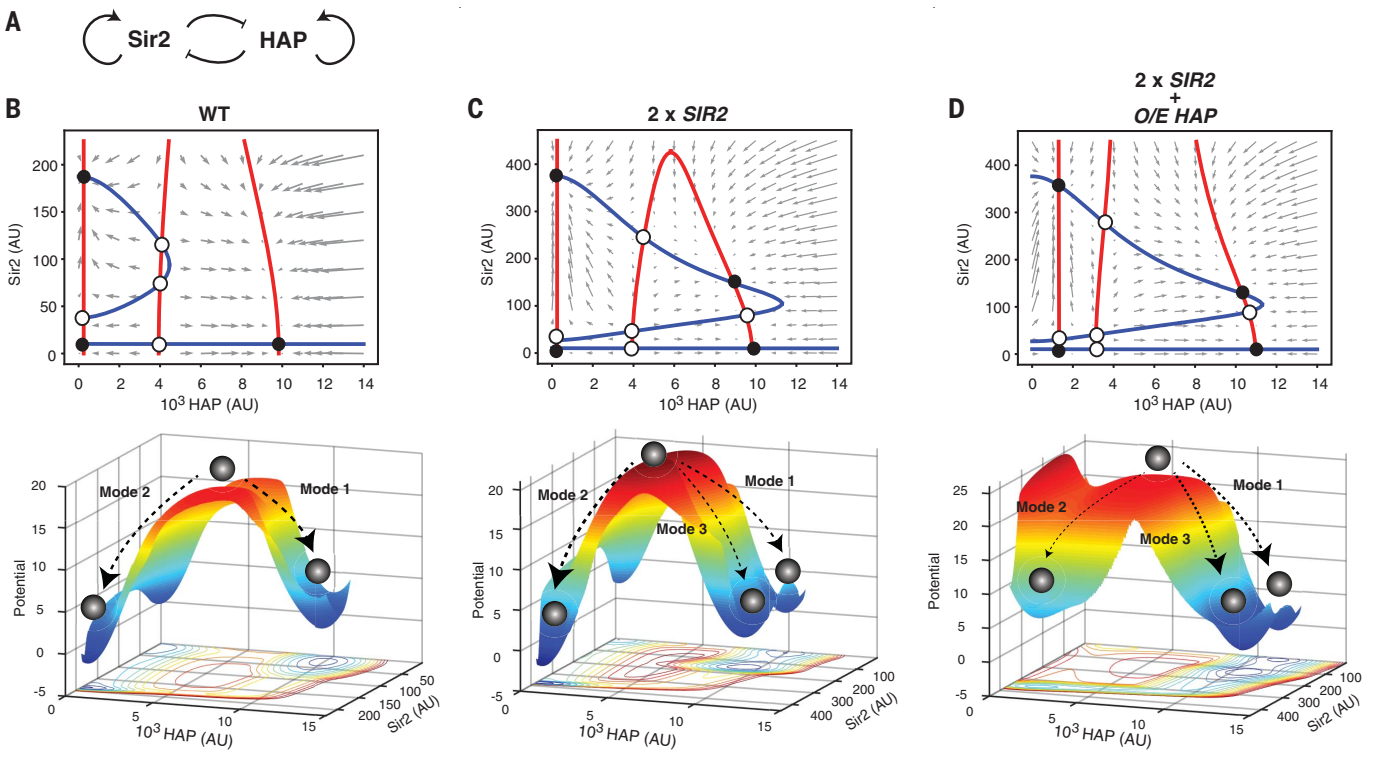

Fig. 3. Computational modeling unravels multistability of the Sir2-HAP circuit that may enable distinct modes of aging. (**A**) The diagram of the circuit topology. Graphic analyses of the model were conducted for (**B**) WT, (**C**) 2 × *SIR2*, and (**D**) 2 × *SIR2* + O/E *HAP* (overexpression). Top panels show phase plane diagrams. The nullclines for Sir2 and HAP are shown in blue and red, respectively. Gray arrows represent the vector field of the system, in which quivers show the rate and direction of movement. Fixed points are indicated with open (unstable) and filled (stable) circles. Bottom panels show computed potential landscapes. Well depths represent the probabilities of cells attracted to them. Single-cell aging processes can be depicted as a ball rolling into one of the wells on the surface.

enhanced in *sir2*Δ (*22*), and, conversely, HAP functions in transcriptional regulation of specific cofactors in Sir2 silencing complexes (*23*–*25*). Positive autoregulation could occur by Sir2 deacetylation of H4-Lys16, creating high-affinity nucleosome binding sites to promote further Sir2 recruitment (*26*–*28*). For positive feedback of HAP, heme activates the HAP complex, leading to increased expression of tricarboxylic acid cycle genes, which, in turn, increases the biosynthesis of heme (*29*). Collectively, this network topology has the potential to generate multistability (*30*).

The dynamical behavior of the system without noise can be analyzed graphically by plotting the nullclines and vector field in a Sir2-HAP phase plane. With appropriate parameters, there are seven fixed points for WT, of which three are stable (Fig. 3B, top). To address the probabilistic nature of single-cell aging, we considered a stochastic version of our model and computed an aging landscape by numerically solving the corresponding two-dimensional Fokker-Planck equation (Fig. 3B, bottom). Each of the stable fixed points of the deterministic system corresponds to a local well on the landscape, with the depth of the well reflecting its fate decision probability. Of the three wells, the deep wells with low Sir2, high HAP or high Sir2, low HAP correspond, respectively, to the experimentally observed mode 1 and mode 2 aging. The low Sir2, low HAP well is shallower (lower probability) and corresponds to a portion of mode 2 cells with low rDNA silencing (Fig. 1G) (see supplementary text section of the supplementary materials; figs. S17 to S21; and tables S1 and S2).

In the model, when the amount of Sir2 was increased twofold, its increased activity partially counteracted the inhibition from HAP, leading to the emergence of a fourth fixed stable point with high Sir2 and high HAP on the phase plane and a new well on the landscape (Fig. 3C), corresponding to experimentally observed mode 3 aging. However, Sir2 overexpression also biases the fate decision toward the high Sir2, low HAP state, consistent with the data indicating that many cells (69.5%) underwent the short-lived mode 2 aging and that the average life span of the whole population was only slightly extended (Fig. 2D). We predicted that an increase in basal HAP abundance under this condition can reshape the landscape to bias toward the high HAP states (Fig. 3D), directing most cells to mode 1 and mode 3 aging and a longer life span.

To test this prediction, we overexpressed both Sir2 and Hap4. Consistent with the model, very few cells (5.8%) underwent mode 2 aging and, instead, many (44.7%) experienced long-lived mode 3 aging (Fig. 4A and fig. S22). The combined perturbation extended the life span more than overexpression of either factor alone (Fig. 4B and table S3) and enabled maintenance of a relatively normal cell cycle length during aging (Fig. 4C). From the network perspective, the combined perturbation can partially neutralize the mutual inhibition between Sir2 and HAP, potentiating a newly observed, distinct long-lived mode with high Sir2 and HAP activities (mode 3) and resulting in a synergistic, rather than additive, effect on lifespan extension (Fig. 4B). A similar effect was observed when we combined the *fob1Δ* long-lived mutant with Hap4 overexpression (fig. S23). This mutant, similar to Sir2 overexpression, enhances rDNA stability. Our model could also help explain the synergy between CR (promoting HAP) and Sir2 (*31*), two seemingly independent longevity factors.

Cellular aging can thus be considered a fate-decision process, in which single cells age toward either silencing loss and nucleolar decline or heme depletion and mitochondrial decline. This process can be viewed as a divergent progression on a Sir2-HAP landscape, which can be reshaped by model-guided genetic

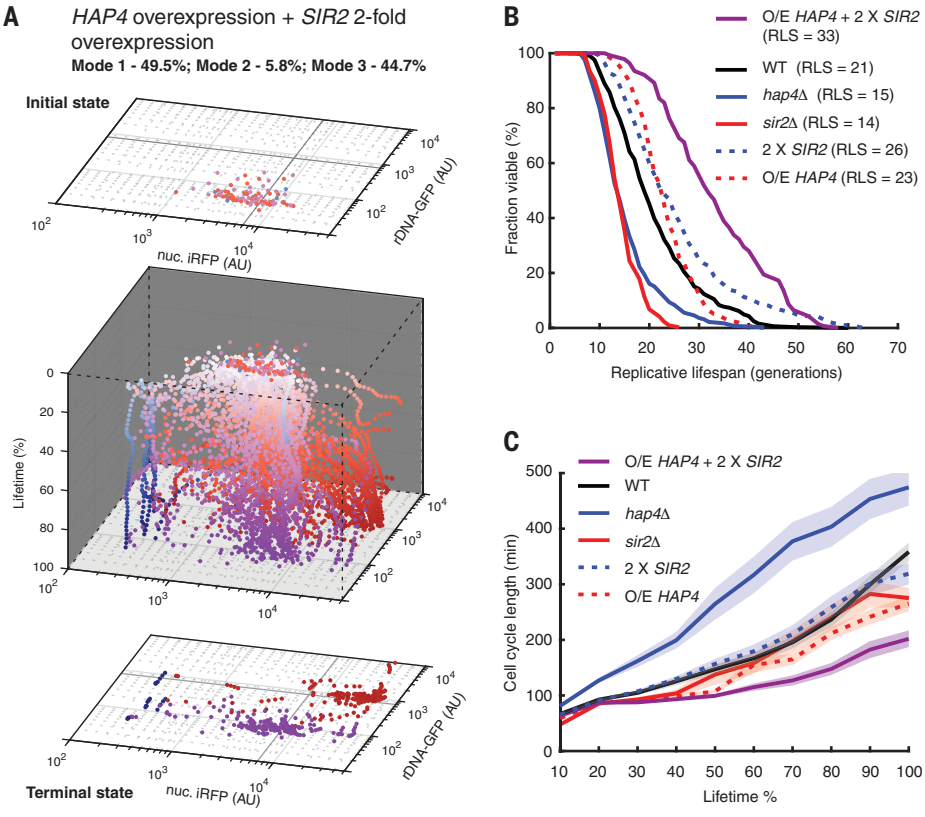

Fig. 4. Combined perturbations of Sir2 and HAP reshape the computed aging landscape and synergistically promote longevity. (**A**) Aging trajectories for the strain with combined *HAP4* overexpression and *SIR2* twofold overexpression (n = 103). Mode 1 cells, red; mode 2 cells, blue; mode 3 cells, purple. (**B**) Replicative life spans for WT, *hap4*Δ, *sir2*Δ, *SIR2* twofold overexpression (2 × *SIR2*), *HAP4* overexpression (O/E *HAP4*), and combined *HAP4* overexpression and *SIR2* twofold overexpression (O/E *HAP4* + 2 × *SIR2*). Significant numbers of life-span changes are included in table S3. (**C**) Changes of cell cycle length during aging for WT, *hap4*Δ, *sir2*Δ, 2 × *SIR2*, O/E *HAP4*, and O/E *HAP4* + 2 × *SIR2*. Shaded areas represent SEM. Experiments were independently performed at least three times.

perturbations, thereby enriching a long-lived mode of aging.

REFERENCES AND NOTES

1. B. K. Kennedy *et al.*, *Cell* **159**, 709–713 (2014).
2. M. M. Crane, M. Kaeberlein, *Curr. Opin. Syst. Biol.* **8**, 25–31 (2018).
3. C. He, C. Zhou, B. K. Kennedy, *Biochim. Biophys. Acta Mol. Basis Dis.* **1864**, 2690–2696 (2018).
4. M. Kaeberlein, *Nature* **464**, 513–519 (2010).
5. K. K. Steffen, B. K. Kennedy, M. Kaeberlein, *J. Vis. Exp.* **2009** 1209 (2009).
6. Y. Li *et al.*, *Proc. Natl. Acad. Sci. U.S.A.* **114**, 11253–11258 (2017).
7. M. Jin *et al.*, *Cell Syst.* **8**, 242–253.e3 (2019).
8. D. A. Sinclair, K. Mills, L. Guarente, *Science* **277**, 1313–1316 (1997).
9. A. L. Hughes, D. E. Gottschling, *Nature* **492**, 261–265 (2012).
10. S. Fehrmann *et al.*, *Cell Rep.* **5**, 1589–1599 (2013).
11. D. A. Sinclair, L. Guarente, *Cell* **91**, 1033–1042 (1997).
12. S. Morlot *et al.*, *Cell Rep.* **28**, 408–422.e4 (2019).
13. M. R. Gartenberg, J. S. Smith, *Genetics* **203**, 1563–1599 (2016).
14. H. Atamna, D. W. Killilea, A. N. Killilea, B. N. Ames, *Proc. Natl. Acad. Sci. U.S.A.* **99**, 14807–14812 (2002).
15. D. A. Hanna *et al.*, *Proc. Natl. Acad. Sci. U.S.A.* **113**, 7539–7544 (2016).
16. G. S. Filonov *et al.*, *Nat. Biotechnol.* **29**, 757–761 (2011).
17. S. Buschlen *et al.*, *Comp. Funct. Genomics* **4**, 37–46 (2003).
18. K. A. Henderson, A. L. Hughes, D. E. Gottschling, *eLife* **3**, e03504 (2014).
19. J. R. Veatch, M. A. McMurray, Z. W. Nelson, D. E. Gottschling, *Cell* **137**, 1247–1258 (2009).
20. S. J. Lin *et al.*, *Nature* **418**, 344–348 (2002).
21. J. L. DeRisi, V. R. Iyer, P. O. Brown, *Science* **278**, 680–686 (1997).
22. A. Ellahi, D. M. Thurtle, J. Rine, *Genetics* **200**, 505–521 (2015).
23. Z. Hu, P. J. Killion, V. R. Iyer, *Nat. Genet.* **39**, 683–687 (2007).
24. J. Reimand, J. M. Vaquerizas, A. E. Todd, J. Vilo, N. M. Luscombe, *Nucleic Acids Res.* **38**, 4768–4777 (2010).
25. M. Becerra *et al.*, *Mol. Microbiol.* **43**, 545–555 (2002).
26. L. Pillus, J. Rine, *Cell* **59**, 637–647 (1989).
27. D. Moazed, *Cell* **146**, 510–518 (2011).
28. K. Sneppen, I. B. Dodd, *Epigenetics* **10**, 293–302 (2015).
29. T. Zhang, P. Bu, J. Zeng, A. Vancura, *J. Biol. Chem.* **292**, 16942–16954 (2017).
30. F. Wu, R. Q. Su, Y. C. Lai, X. Wang, *eLife* **6**, e23702 (2017).
31. M. Kaeberlein, K. T. Kirkland, S. Fields, B. K. Kennedy, *PLOS Biol.* **2**, e296 (2004).
32. yaj030, yaj030/aging_science2020 v1.1, Version 1.1,Zenodo (2020); http://doi.org/10.5281/zenodo.3770529.

ACKNOWLEDGMENTS

We thank G. Zhu for help with image analysis, A. R. Reddi (Georgia Tech) and D. E. Gottschling (Calico) for generously providing strains and reagents, and E. L. Petty for guidance with CNV analysis. **Funding:** This work was supported by the National Institutes of Health, National Institute on Aging, AG056440 (to N.H., J.H., L.P., and L.S.T.); NSF MCB-1616127 (N.H.); and NSF MCB-1716841 (L.P.). **Author contributions:** Conceptualization, Y.L., Y.J., L.P., L.S.T., J.H., and N.H.; Methodology, Y.L., Y.J., R.O., and S.K.; Investigation, Y.L., J.P., and S.K.; Formal Analysis, Y.L., Y.J., Y.Z., and L.S.T.; Writing – Original Draft, Y.L., Y.J., and N.H.; Writing – Review & Editing, Y.L., Y.J., J.P., R.O., L.P., L.S.T., J.H., and N.H.; Resources, L.P., L.S.T., J.H., and N.H.; Funding Acquisition, L.P., L.S.T., J.H., and N.H.; Supervision, N.H.; Project Administration, N.H. **Competing interests:** J.H. is a founder of GenCirq and Quantitative BioSciences, which focus on cancer therapeutics and agricultural synthetic biology, respectively; there is no competing interest with this work. The other authors also declare no competing interests. **Data and materials availability:** All data are available in the main text or the supplementary materials. The code from this work is available at https://github.com/yaj030/aging_science2020 and Zenodo (*32*).

SUPPLEMENTARY MATERIALS

science.sciencemag.org/content/369/6501/325/suppl/DC1
Materials and Methods
Supplementary Text
Figs. S1 to S23
Tables S1 to S6
References (*33*–*37*)
MDAR Reproducibility Checklist
Movies S1 and S2

7 May 2019; resubmitted 24 January 2020
Accepted 13 May 2020
10.1126/science.aax9552

Science

A programmable fate decision landscape underlies single-cell aging in yeast

Yang Li, Yanfei Jiang, Julie Paxman, Richard O'Laughlin, Stephen Klepin, Yuelian Zhu, Lorraine Pillus, Lev S. Tsimring, Jeff Hasty and Nan Hao

Science **369** (6501), 325-329.
DOI: 10.1126/science.aax9552

Programmed aging in yeast cells

Following the fate of individual yeast cells has revealed aging to be more of a programmable decision process rather than a simple accumulation of deleterious events. Li *et al.* combined single-cell studies and mathematical modeling to show that yeast cells showed two different forms of aging: one with more ribosomal DNA silencing, in which nucleoli were degraded, and another with more heme accumulation and hemedependent transcription, in which mitochondria were more affected. Overexpression of the lysine deacetylase Sir2, which contributes to ribosomal DNA silencing, led to a third cell-aging fate in which the average life span was extended. If other cells age in similar ways, then this study may provide new ways to consider dynamics of aging and strategies to extend the health span.

Science this issue p. 325